# A COMPREHENSIVE STUDY ON OPTICAL FEATURES, GAMMA PHOTON BUILDUP FACTORS AND NEUTRON SHIELDING CAPABILITY OF $B_2O_3$-$SB_2O_3$-$LI_2O$-$BI_2O_3$ GLASSES

Norah A.M. Alsaif[1], A.M. Abdelghany[2,*], Y.S. Rammah[3], I.O. Olarinoye[4], N.V. Kudrevatykh[5] and A.S. Abouhaswa[3,5]

[1]Department of Physics, College of Science, Princess Nourah bint Abdulrahman University, Riyadh, Saudi Arabia
[2]Spectroscopy Department, National Research Centre, 33 Elbehouth St., Dokki, 12622 Cairo, Egypt
[3]Department of Physics, Faculty of Science, Menoufia University, 32511 Shebin El Koom, Egypt
[4]Department of Physics, School of Physical Sciences, Federal University of Technology, Minna, Nigeria
[5]Ural Federal University, 19 Mira St, 620002, Yekaterinburg, Russia

**ABSTRACT**. Linear, nonlinear optical properties, photon buildup factors, and neutron shielding capability of glasses with chemical composition $(65-x)B_2O_3$-$10Sb_2O_3$-$25Li_2O$-$xBi_2O_3$, where x = 0 (BSLB0) – 20 (BSLB20) mol% with steps of 4 mol% were examined. Molar refractivity ($R^{molar}$) and molar polarizability ($\alpha^{molar}$) were increased as $Bi_2O_3$ content mol% increase in the examined BSLB-glasses. The values of metallization criterion ($M^{criterion}$) confirmed that the BSLB-glasses were non-metallic materials. The static ($\varepsilon^{static}$) and optical ($\varepsilon^{optical}$) dielectric constants having the same trend of the refractive index ($n^{optical}$). Values of optical electronegativity ($\chi^*$) were reduced from 0.825 for BSLB0 ($Bi_2O_3$ = 0 mol%) glasses to 0.758 for BSLB20 ($Bi_2O_3$ = 20 mol%) glasses. The linear electric/dielectric susceptibility ($\chi^{(1)}$) increased from 0.370 to 0.397. The nonlinear optical susceptibility ($\chi^3$) and nonlinear refractive index $n_2^{optical}$ were enhanced by increasing $Bi_2O_3$ content in the BSLB-glasses. The BSLB20 glasses presented the least exposure and energy absorption build-up factors (EBF and EABF) at all considered thickness. BSLB20 sample achieved the best fast neutron removal cross section ($\Sigma_R$) shield among all glasses. The total stopping powers (TSP) follows the trend $(TSP)_{BSLB0} < (TSP)_{BSLB4} < (TSP)_{BSLB8} < (TSP)_{BSLB12} < (TSP)_{BSLB16} < (TSP)_{BSLB20}$. The electron absorbing and hence shielding capacity of the BSLB-glasses improves as their $Bi_2O_3$ content increase.

**KEY WORDS**: Antimony lithium-borate glasses, Optical properties, Buildup factors, Neutron shielding

## INTRODUCTION

Many scientists are paying more attention to the linear and nonlinear optical properties of transparent materials (glasses). These characteristics aid in the selection of appropriate glasses for specific applications [1-11]. Boron-based glasses are one of the most interesting glasses because of their unique physical properties, which include low cost, ease of preparation, low glass transition temperature, high refractive index, good thermal stability, and higher optical transmission in the infrared region [1, 2].

Ionizing radiation emitted by various radiation isotopes and machines is used in a variety of nuclear technologies [12, 13]. In recent years, nuclear technology has been used in environmental conservation, power generation, consumer goods, medicine, scientific research, agriculture, and food processing industries [12, 14, 15]. Furthermore, one of the primary goals of high radiation protection efficiency (RPE) has been to find radiation shields with more appropriate properties [3-8, 12-15].

_____

*Corresponding author. E-mail: a.m_abdeghany@ yahoo.com

In most applications, radiation shields must be optically transparent, recyclable, environmentally friendly, durable, and have high mechanical, thermal, and mechanical stability [5, 12-15]. Several authors [16-21] have been fabricated glasses to meet these specifications because several traditional shielding materials do not authenticate some of these requirements. As a result, there has been a significant increase in research into the preparation of glass systems for use in radiation protection and nuclear technology [22-29].

Borate-based glasses are inexpensive and have excellent mechanical, thermal, optical, and electrical properties, making them useful in nuclear optical and radiation protection applications [4-6, 13]. Furthermore, adding metal oxide glass modifiers to the glass system, such as $Bi_2O_3$, $Li_2O$, $ZnO$, $CaO$, $Al_2O_3$, and $CdO$, allows the produced glasses to be used in a variety of applications [2-4, 23]. Glasses made by mixing $Bi_2O_3$ into a glass matrix have a high density, a high refractive index, a low crystallisation rate, radiation tolerance, and an increase in other properties [8]. Furthermore, because $Bi_2O_3$ glasses have a higher photon absorption coefficient than other glasses, they have a higher radiation shielding efficiency. As a result, borate glasses containing $Bi_2O_3$ could be used as X- and gamma-ray shielding materials. Abouhaswa *et al.* [30] studied the structural, optical, and gamma-ray shielding characteristics of antimony lithium-borate with bismuth glasses. They reported that the enhancement of $Bi_2O_3$ content in the mentioned glasses leads to decrease of the optical energy gap and increase the refractive index. In terms of radiation protection issue, the capacity of glasses as radiation shielding increased as $Bi_2O_3$ content increase in glasses.

The main goal of this research is to look into the linear and nonlinear optical properties of antimony lithium-borate glasses of composition $B_2O_3$-$Sb_2O_3$-$Li_2O$-$Bi_2O_3$ as well as photon (exposure and energy absorption) build-up factors, and neutron shielding capability of these glasses have been examined. To this end, several of optical characteristics such as molar refractivity, molar polarizability, dielectric constants, electronegativity, nonlinear optical susceptibility, and nonlinear optical refractive index were investigated. Furthermore, gamma-ray build-up factors, the total stopping powers (TSP), and range of the continuous slowing down approximation (CSDA) of glasses were evaluated in order to investigate their uncharged and charged particles shielding efficacy.

## EXPERIMENTAL

### Procedure

The studied antimony lithium-borate glasses of compositions of $(65-x)B_2O_3$-$10Sb_2O_3$-$25Li_2O$-$xBi_2O_3$, where x = 0-20 mol percent with steps of 4 mol percent were fabricated using a traditional solid-state process. More information on the fabrication processes can be found in our previous work [30]. The studied glasses were given the same codes as in [30], namely BSLB-glasses in general and BSLB0 (x = 0), BSLB4 (x = 4), BSLB8 (x = 8), BSLB12 (x = 12), BSLB16 (x = 16), and BSLB20 (x = 20). Table 1 lists the sample codes, chemical compositions, density, and molar volume of the studied BSLB-glasses.

Table 1. Sample code, density, and molar volume of antimony lithium-borate glasses $(65-x)B_2O_3$ -$10Sb_2O_3$ - $25Li_2O$ - $xBi_2O_3$ x = 0, 4, 8, 12, 16, and 20 mol%.

| Sample | Chemical composition [30] | Density g/cm$^3$ [30] | Molar volume (cm$^3$/mol) [30] |
|--------|---------------------------|----------------------|-------------------------------|
| BSLB0 | $65B_2O_3$ - $10Sb_2O_3$ - $25Li_2O$ - $0Bi_2O_3$ | 2.7125 | 30.1843 |
| BSLB4 | $61B_2O_3$ - $10Sb_2O_3$ - $25Li_2O$ - $4Bi_2O_3$ | 2.9951 | 32.6295 |
| BSLB8 | $57B_2O_3$ - $10Sb_2O_3$ - $25Li_2O$ - $8Bi_2O_3$ | 3.1524 | 36.0304 |
| BSLB12 | $53B_2O_3$ - $10Sb_2O_3$ - $25Li_2O$ - $12Bi_2O_3$ | 3.4925 | 37.0611 |
| BSLB16 | $49B_2O_3$ - $10Sb_2O_3$ - $25Li_2O$ - $16Bi_2O_3$ | 3.6554 | 39.7465 |
| BSLB20 | $45B_2O_3$ - $10Sb_2O_3$ - $25Li_2O$ - $20Bi_2O_3$ | 3.9454 | 40.8433 |

*Linear/nonlinear optical properties*

In this study, with the help of the optical energy band gap ($E^{optical}$) and refractive index ($n^{optical}$) of the BSLB-glasses which estimated experimentally in our previous work [30], linear and nonlinear optical properties are calculated as in Equations (1-13) [31-34]: Molar refractivity,

$$\text{Molar refractivity, } R^{molar} = \left( \frac{(n^{optical})^2 - 1}{(n^{optical})^2 + 2} \right) V^{molar} \tag{1}$$

where $V^{molar}$ is the molar volume of glasses.

$$\text{Molar polarizability, } \alpha^{molar} = \frac{R^{molar}}{2.52} \tag{2}$$

$$\text{Reflection loss, } R^{loss} = \left( \frac{(n^{optical}) - 1}{(n^{optical}) + 1} \right)^2 \tag{3}$$

$$\text{Optical transmission, } T^{optical} = \frac{2(n^{optical})}{(n^{optical})^2 + 1} \tag{4}$$

$$\text{Metallization criterion, } M^{criterion} = 1 - \frac{R^{molar}}{V^{molar}} \tag{5}$$

$$\text{Static dielectric constant, } \varepsilon^{static} = (n^{optical})^2 \tag{6}$$

$$\text{Optical dielectric constant, } \varepsilon^{optical} = \varepsilon^{static} - 1 = \left( n^{optical} \right)^2 - 1 \tag{7}$$

$$\text{Refractive index-based metallization criterion, } M(n^{optical}) = 1 - \left( \frac{(n^{optical})^2 - 1}{(n^{optical})^2 + 2} \right) \tag{8}$$

$$\text{Optical energy band gap-based metallization criterion, } M(E^{optical}) = \left( \frac{E^{optical}}{20} \right)^{1/2} \tag{9}$$

$$\text{Optical electronegativity, } \chi^* = 0.2688 E^{optical} \tag{10}$$

$$\text{Linear electric/dielectric susceptibility, } \chi^{(1)} = ((n^{optical})^2 - 1)/4\pi \tag{11}$$

$$\text{Nonlinear optical susceptibility, } \chi^3 (esu) = A/(4\pi)^4 (n^{optical} - 1)^4 \tag{12}$$

Where A= $1.7 \times 10^{-10}$ is a constant.

$$\text{Non-linear refractive index, } n_2^{optical} (esu) = \frac{12\pi \chi^3}{n^{optical}} \tag{13}$$

*Photon buildup factors*

As is well established, the Beer-Lambert expression can be used to measure the photon absorption potential of any substance by simulation and experimentation:

$$I = I_o \exp(-\mu t) \tag{14}$$

where $I$ and $I_o$ reflect the transmitted and incident photon flux through the substance of mass thickness t (g/cm$^2$), respectively. The linear attenuation coefficient ($\mu$ = LAC) of the absorber is defined as (cm$^{-1}$). When the transmitted photon flux consists of both primary (un-collided) and secondary (scattered) photons, expression (14) becomes:

$$I = BFI_o \exp(-\mu t) \tag{15}$$

When the transmitted beam does not contain scattered photons, the photon buildup factor (BF) of the photon flux is equal to unity. BF has been the subject of detailed reports elsewhere [35-38]. The fraction of incident photons transmitted through the attenuator is determined by the photon transmission factor (TF). If the BF is considered, theoretically, TF is expressed as:

$$T(E, \mu t) = \frac{I}{I_o} = BF(E, \mu t) \text{xp}(-\mu t) \tag{16}$$

The EXABCal computer code was used to measure exposure (EBF) and energy absorption (EABF) BF in the BSLB-glasses for selected depths up to 40 MFP in this study [36].

*Fast neutron macroscopic removal cross-section ($\Sigma_R$)*

The neutron absorption efficacy of a material is generally described by appropriate microscopic and macroscopic cross-sections of the neutron beam. Unlike photons, neutrons are classified into energy groups such as fast, intermediate, and thermal neutrons. Microscopic and macroscopic cross-sections of neutrons differ and depend on the class/energy of neutrons of interest. For fast neutrons, the fast neutron removal cross-section ($FNRC - \Sigma_R$) is the macroscopic cross-section for fissile neutrons, while the microscopic scattering and absorption cross-section may be adopted for thermal neutron shielding parameter. $FNR$ for the glasses under study were calculated via the equation [39, 40]:

$$\Sigma_R = \rho \sum w_i \left(\frac{\Sigma_R}{\rho}\right)_i \tag{17}$$

where, $w_i$, and $\left(\frac{\Sigma_R}{\rho}\right)_i$ are the mass density, weight fraction, and mass removal cross-section of the $i^{th}$ element of the glass, respectively. $\frac{\Sigma_R}{\rho}$ for each constituent element was calculated using their atomic numbers, $Z$ as given in equations 18a and b.

$$\frac{\Sigma_R}{\rho} = 0.19 Z^{-0.743} \quad \text{for } Z \leq 8; \tag{18a}$$

and,

$$\frac{\Sigma_R}{\rho} = 0.125 Z^{-0.565} \text{ for } Z > 8 \tag{18b}$$

Total macroscopic cross-section $\Sigma_T$ (cm$^{-1}$) for thermal neutrons of the glasses was calculated through the equation [41-43]:

$$\Sigma_T = 6.02 \times 10^{23} \rho \sum_i \frac{w_i}{M_i} (\sigma_T)_i \tag{19}$$

where, $\sigma_T$ (cm$^2$) is the total microscopic cross-section (sum of absorption and scattering cross-sections).

*Stopping powers (MSP) and projected range (R) of ions*

The stopping power of a charged particle travelling through a substance is the average energy lost by the particle (SP). The coulomb interaction with the orbital electrons of atoms in the substance (electronic loss) or with the atomic nuclei causes the majority of the energy loss (nuclear loss). For protons, total SP includes both electronic and nuclear losses, whereas for electrons, total SP includes both electronic and radiative losses. The ESTAR software [44] was used to determine the total SP and CSDA range (R) of electrons in the selected glasses.

## RESULTS AND DISCUSSION

*Linear/nonlinear optical parameters*

The variation of both ($R^{molar}$) and ($\alpha^{molar}$) with the changing of $Bi_2O_3$ content mol% in the synthesized BSLB0- BSLB20 glasses are depicted in Figure 1(a) and (b), respectively and Table 2. It was noticed that the values of ($R^{molar}$) are directly related to the values of ($\alpha^{molar}$), and both are increasing with the increase of $Bi_2O_3$ content mol%. This variation may be due to the increase of $Bi_2O_3$ content in the glass composition, causes the breaking in the regular structure of antimony lithium-borate glasses and raising the number of non-bridging oxygens (NBO) atoms leading to a decrease in the $E^{optical}$ value as in Table 2.

Values of the ($T^{optical}$) and ($R^{loss}$) with the increasing of $Bi_2O_3$ content mol% in the studied BSLB0- BSLB20 glasses are collected in Table 2. It was observed that these parameters were in an inverse relationship due to the increase in the number of (NBO) atoms. The obtained values of ($M^{criterion}$), ($\varepsilon^{static}$), and ($\varepsilon^{optical}$) with $Bi_2O_3$ content mol percent in the studied BSLB0- BSLB20 glasses are listed in Table 2. The ($M^{criterion}$) ranged from 0.300 to 0.286, indicating that the samples under consideration are appropriate for nonlinear optical applications. Also, as shown in Tables 1 and 2, the values of ($M^{criterion}$) confirm that the BSLB-glasses are non-metallic materials since their ($R^{molar}$) values are less than those of ($V^{molar}$) [32]. Furthermore, as shown in Table 2, the ($\varepsilon^{static}$), ($\varepsilon^{optical}$), and refractive index ($n^{optical}$) have the same pattern.
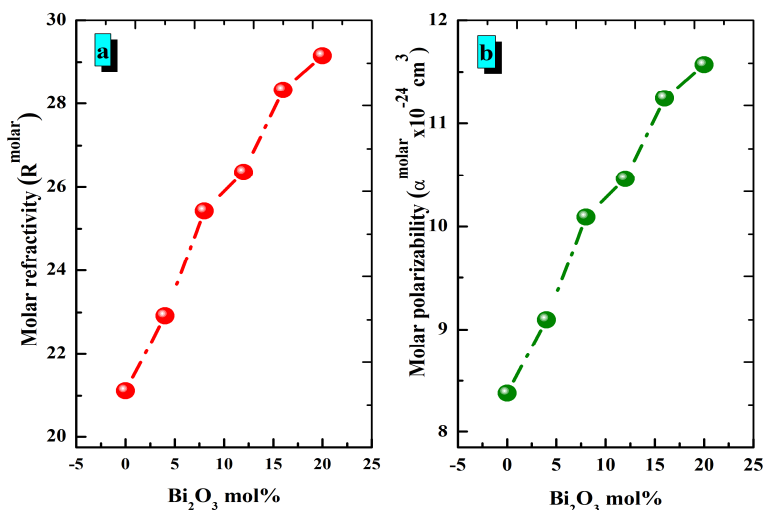


Figure 1. Variation of $R^{molar}$ (a) $\alpha^{molar}$ (b) with $Bi_2O_3$ content mol% of the investigated BSLB-glasses.

Table 2. The obtained values of $E^{optical}$, $n^{optical}$, $R^{molar}$, $\alpha^{molar}$, $R^{loss}$, $T^{optical}$, $M^{criterion}$, $\varepsilon^{static}$, $\varepsilon^{optical}$, M(n), M($E^{optical}$), ($\chi^*$), ($\chi^{(1)}$), ($\chi^3$), and ($n_2^{optical}$) of the studied glasses.

| Physical parameter | Sample code | | | | | |
|---|---|---|---|---|---|---|
| | BSLB0 | BSLB4 | BSLB8 | BSLB12 | BSLB16 | BSLB20 |
| $E^{optical}$ (eV) $\pm$ 0.01 [30] | 2.63 | 2.58 | 2.54 | 2.50 | 2.47 | 2.45 |
| $n^{optical}$ $\pm$ 0.01 [30] | 2.50 | 2.52 | 2.53 | 2.54 | 2.55 | 2.56 |
| $R^{molar}$ (cm$^3$/mol) $\pm$ 0.001 P.W$^*$ | 21.116 | 22.918 | 25.430 | 26.370 | 28.327 | 29.156 |
| $\alpha^{molar}$ x10$^{-24}$ cm$^3$ $\pm$ 0.001 P.W$^*$ | 8.379 | 9.094 | 10.091 | 10.464 | 11.240 | 11.569 |
| $R^{loss}$ $\pm$ 0.001 P.W$^*$ | 0.166 | 0.168 | 0.170 | 0.174 | 0.175 | 0.176 |
| $T^{optical}$ $\pm$ 0.001 P.W$^*$ | 0.714 | 0.711 | 0.708 | 0.702 | 0.701 | 0.700 |
| $M^{criterion}$ $\pm$ 0.001 P.W$^*$ | 0.300 | 0.297 | 0.294 | 0.288 | 0.287 | 0.286 |
| $\varepsilon^{static}$ $\pm$ 0.001 P.W$^*$ | 5.657 | 5.720 | 5.798 | 5.933 | 5.961 | 5.989 |
| $\varepsilon^{optical}$ $\pm$ 0.001 P.W$^*$ | 4.657 | 4.720 | 4.798 | 4.933 | 4.961 | 4.989 |
| M(n) $\pm$ 0.001 P.W$^*$ | 0.391 | 0.388 | 0.384 | 0.378 | 0.376 | 0.375 |
| M($E^{optical}$) $\pm$ 0.001 P.W$^*$ | 0.076 | 0.075 | 0.074 | 0.072 | 0.071 | 0.070 |
| ($\chi^*$) $\pm$ 0.001 P.W$^*$ | 0.825 | 0.811 | 0.795 | 0.768 | 0.763 | 0.758 |
| ($\chi^{(1)}$) $\pm$ 0.001 P.W$*$ | 0.370 | 0.375 | 0.382 | 0.392 | 0.394 | 0.397 |
| ($\chi^3$) x 10$^{-12}$ (esu) $\pm$ 0.001 P.W$^*$ | 3.213 | 3.391 | 3.620 | 4.046 | 4.138 | 4.233 |
| ($n_2^{optical}$) x10$^{-10}$ (esu) $\pm$ 0.001 P.W$^*$ | 5.090 | 5.342 | 5.665 | 6.258 | 6.386 | 6.517 |

P.W$^*$ = Present work.

The effect of $Bi_2O_3$ content mol percent on the M($E^{optical}$) and M($n^{optical}$) of the BSLB0-BSLB20 glasses depicts as values in Table 2. These two optical parameters have the same pattern, i.e., they decreased as the $Bi_2O_3$ content in the glasses increased.

The variation of the optical electronegativity ($\chi^*$) and the linear dielectric susceptibility $\chi^{(1)}$ with $Bi_2O_3$ content mol% in the BSLB0-BSLB20 glasses is shown in Table 2. As shown in Table 2, the value of $\chi^*$ reduces from 0.825 for BSLB0 ($Bi_2O_3$ = 0 mol%) glasses to 0.758 for BSLB20 ($Bi_2O_3$ = 20 mol%) glasses, while $\chi^{(1)}$ increases from 0.370 to 0.397. These trends attributed to the increasing number of non-bridging oxygen (NBO) atoms in the investigated BSLB0- BSLB20 glass's framework.

Finally, Figure 2 shows the variation of the nonlinear optical susceptibility, $\chi^3$ (a) and nonlinear refractive index, $n_2^{optical}$ (b) for the investigated BSLB-glasses. As shown from Figure 2 and its corresponding data in Table 2, both ($\chi^3$) and $n_2^{optical}$ were enhanced with the increase of $Bi_2O_3$ content in the investigated BSLB0- BSLB20 glasses. This enhancement may be due to the increasing number of non-bridging oxygen (NBO) atoms in the glass's framework.

*Photon buildup factors*

Exposure (EBF) and energy absorption (EABF) buildup factors (BF) of the investigated BSLB-glasses and their variations with respect to photon energies (0.15–15 MeV) and selected penetration depths up to 40 MFP are presented in Figure 3 for BSLB0 sample and Figure 4 for BSLB20 glasses, respectively. According to the figures, the changes in the BF values with energy are similar for all the glasses except with the peak values at absorption edges which is a function of the chemical composition of the glasses. The partial PA, CS, and PP interaction modes play a major role in the behavior of the build-up factors. Generally, BF values were comparatively lowest in the PA dominated energies safe for absorption edges. On the other hand, values of BF were also lower in the PP dominated energies than the CS energies. Partial CS interaction leads to photon buildup while PA and PP processes absorb the photon and lower build-ups at energies where PA and PP dominate [36]. Comparing the BF of the glasses at two energies; 0.1 MeV (Figure 5) and 1 MeV (Figure not shown here) and different depths is performed. At both energies,

both EABF and EBF increase in values as the thickness (in MFP) of the BSLB-glasses increase; an indication that photons suffer more collisions within the interacting glass medium. Hence the number of photons with lower energy compared to the incident photon energy increase (buildup). Also observed is the fact that at the photon energy of 0.1 MeV, the highest BF was found in BSLB0 glasses while the least was obtained for BSLB12 glasses. For the 1 MeV spectra, the least BF was found for BSLB20 with BSLB4 glasses having the highest. This shows that relative values of BF vary with energy; however, as energy progresses, the BSLB20 glasses presented the least BF at all considered thickness. Considering all the calculated photon interaction parameters, it is obvious that the increase in the Bi content of glasses improves their photon absorption and protection abilities.
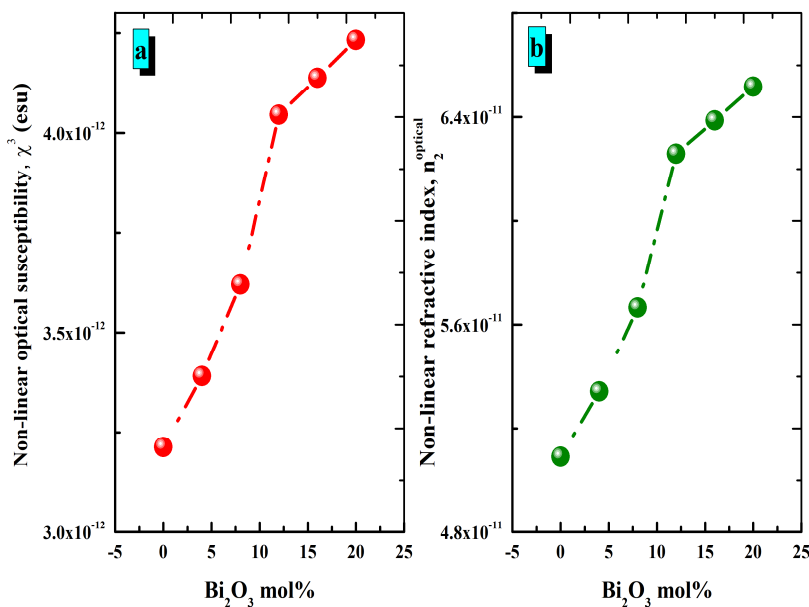


Figure 2. Variation of $\chi^3$ (a) and (b) $n_2{}^{optical}$ with the investigated BSLB-glasses.

*Fast neutron macroscopic removal cross-section ($\Sigma_R$)*

The calculated values of $\Sigma_R$ for BSLB-glasses varied from 0.1265–0.1584 cm$^{-1}$ as the Bi$_2$O$_3$ of the glass system increased from 0–20 wt%. This shows consistent growth in the fast neutron removal capacity of the glasses. This is attributed to the growth in partial densities of B and Li in the glasses. These two elements have comparatively higher fast neutron removal cross-sections than other elements present in the glass systems. Based on the $\Sigma_R$ results, the best fast neutron shield among the glasses is BSLB20. A comparison of the $\Sigma_R$ of water, OC [45] and recently studied glasses (80TeO$_2$.20BaO (TB), 80TeO$_2$.20ZnO (TZ), TVB25 and TVM60) [25, 46-48] and BSLB20 is depicted in Figure 6. This shows that the value of $\Sigma_R$ for BSLB20 higher than these others and a preferred fast neutron shield compared with these materials.
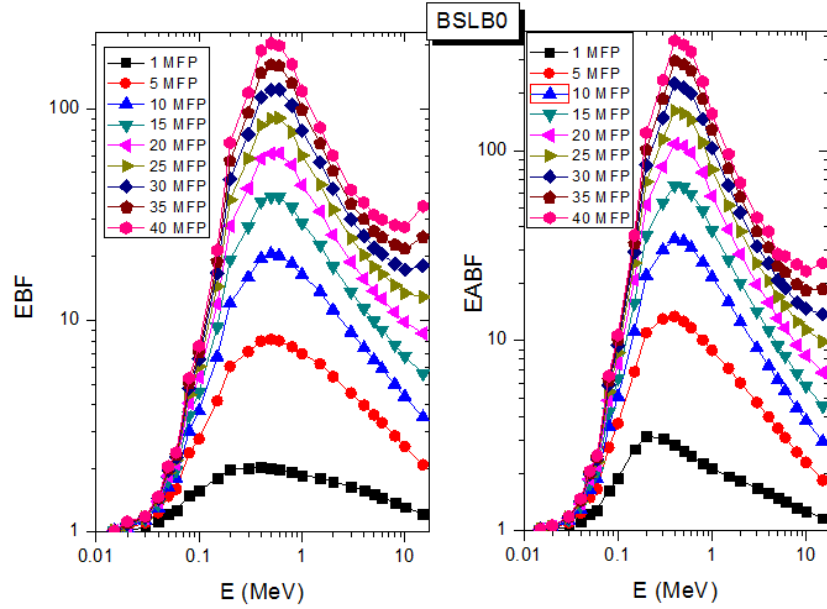
Norah A.M. Alsaif *et al.*



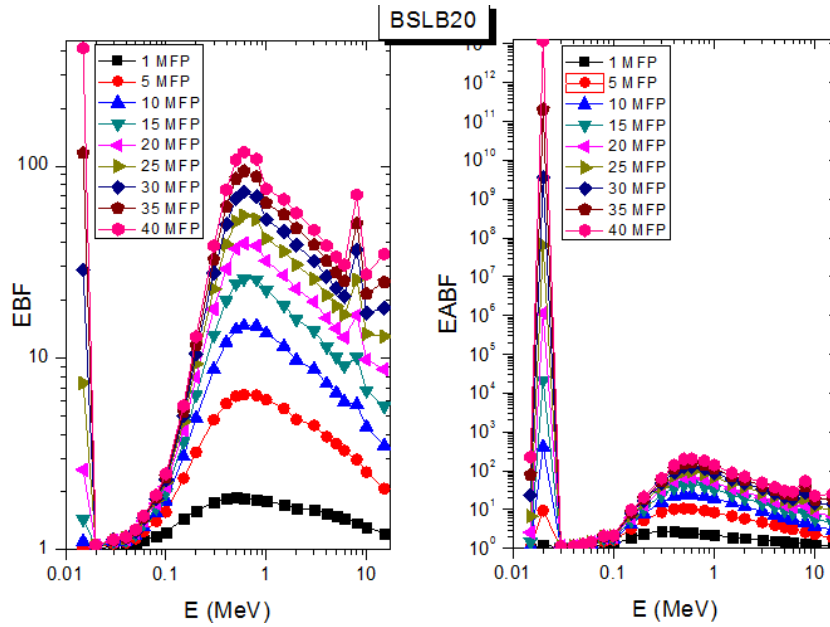Figure 3. EBF and EABF spectra of BSLB0 glass at different penetration depths.



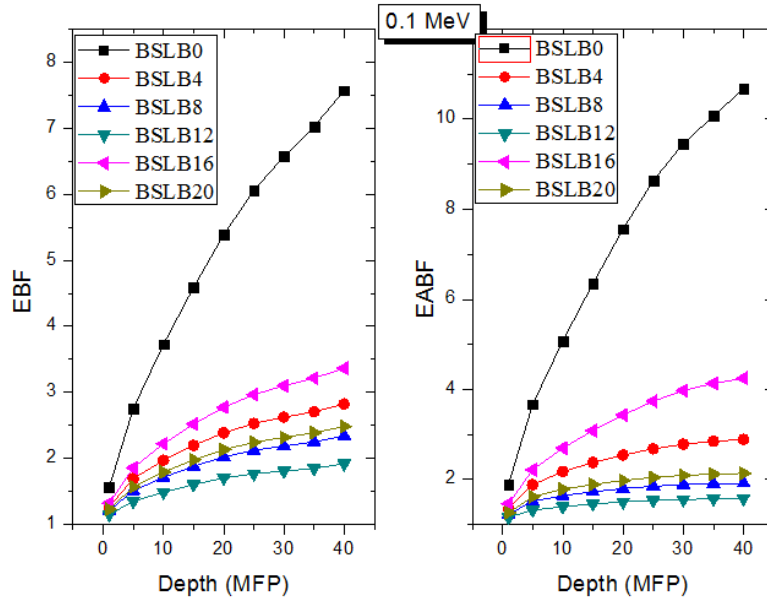Figure 4. EBF and EABF spectra of BSLB20 glass at different penetration depths.

Figure 5. EBF and EABF variation with penetration depth for the BSLB-glasses at 0.1 MeV.
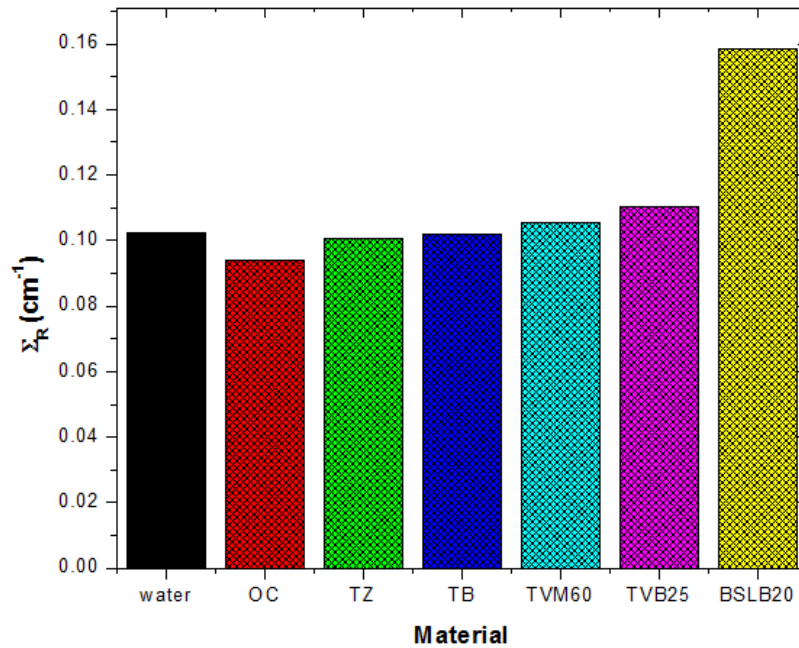


Figure 6. A comparison of the $\Sigma_R$ of BSLB20 glasses and other materials.

*Total stopping powers (TSP) and CSDA-Range of electrons in the glass system*

The total stopping powers (TSP) and range of the continuous slowing down approximation (CSDA) of the BSLB-glasses were evaluated in order to investigate their charged particle shielding efficacy. Figure 7 and Figure 8 show the variance of the glasses' TSP and CSDA ranges as a function of electron kinetic energy up to 15 MeV, respectively. In general, as the electron's kinetic energy increases, the TSP of the electron in the glasses decreases at first, then increases slightly. Changes in partial stopping powers caused by electron collision and radiation are thought to be the cause of this action. The collision stopping power (CSP) dominated the TSP of the electron in the glasses below 1 MeV, while the radiative stopping power (RSP) dominated above this energy. With increasing electron kinetic energy, CSP typically decreases while RSP increases, resulting in the observed behavior of the TSP spectra of the glasses. The TSP fits the pattern $(TSP)_{BSLB0} < (TSP)_{BSLB4} < (TSP)_{BSLB8} < (TSP)_{BSLB12} < (TSP)_{BSLB16} < (TSP)_{BSLB20}$ across the entire kinetic energy continuum. The electron's TSP is usually directly proportional to the electron density (Na) of the interacting medium [49]:

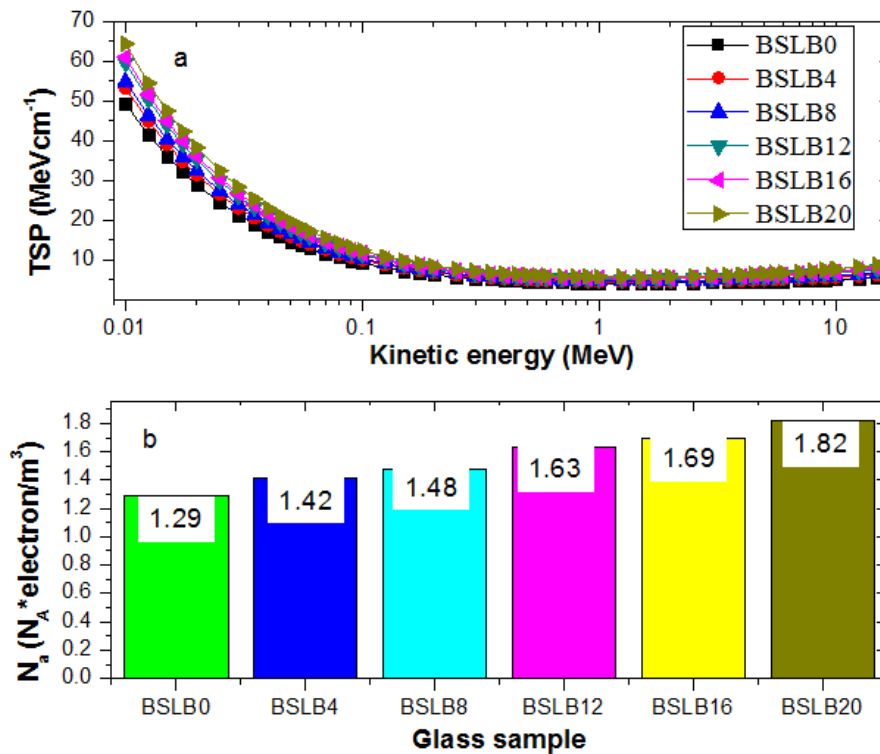$$TSP \propto N_a = \rho N_A \frac{Z}{A} \tag{20}$$



Figure 7. Variation of TSP of electron as a function of kinetic energy (a) and $N_a$ of the glasses.
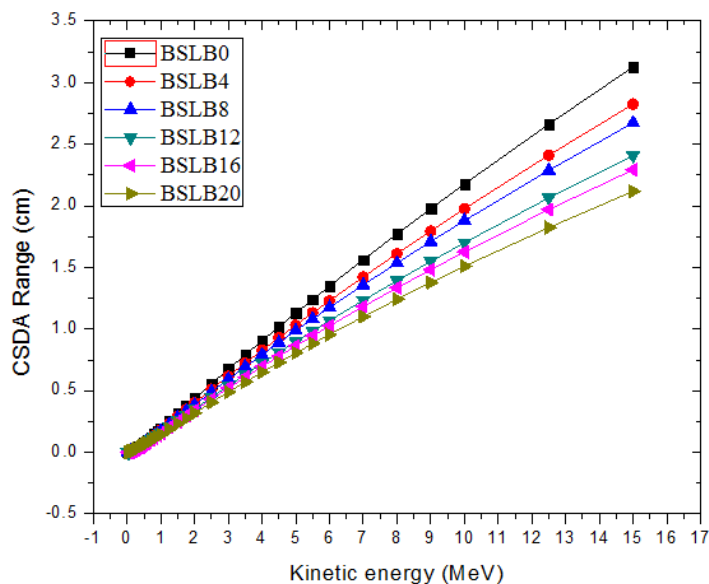
Figure 8. Variation of CSDA range of electron in the BSLB-glasses as a function of kinetic energy.

The Na (Figure 7b) is arranged in the same order as TSP (Figure 7a). This helps to understand why the electron's TSP was highest in the BSLB20 glass study. In addition, Figure 8 shows that the CSDA range of all glasses increases as the electron's kinetic energy increases. Higher-energy particles have a faster velocity and can therefore travel further than lower-energy particles; this explains the observed range trend. The distribution follows the opposite pattern as TSP, so the highest electron range was found in BSLB0 glasses and the lowest in BSLB20 glasses. Since the electron loses more energy in the BSLB20 sample than in the rest glasses, it comes to rest at a lower depth inside the bottle, as shown. As the $Bi_2O_3$ content of the BSLB-glasses increases, so does their electron absorption and thus shielding ability.

## CONCLUSION

The present study aimed to investigate the linear, nonlinear optical properties, the photon build-up factors, and neutron shielding capability of antimony lithium-borate reinforced with $Bi_2O_3$ with chemical composition $(65-x)B_2O_3-10Sb_2O_3-25Li_2O-xBi_2O_3$, where x = 0-20 mol% with steps of 4 mol%. Results revealed that: Values of ($R^{molar}$) are in direct relation with the values of ($\alpha^{molar}$) and both were increasing with the increase of $Bi_2O_3$ content mol% in the examined BSLB-glasses. The ($T^{optical}$) and ($R^{loss}$) were in an inverse relationship due to the increase in the number of (NBOs) atoms in glass's framework. The values of ($M^{criterion}$) confirm that the BSLB-glasses are non-metallic materials and the ($\varepsilon^{static}$) and ($\varepsilon^{optical}$) having the same trend of the refractive index ($n^{optical}$). Value of $\chi^*$ reduces from 0.825 for BSLB0 ($Bi_2O_3$ = 0 mol%) glasses to 0.758 for BSLB20 ($Bi_2O_3$ = 20 mol%) glasses, while $\chi^{(1)}$ increases from 0.370 to 0.397. Both $\chi^3$ and $n_2^{optical}$ were enhanced with the increase of $Bi_2O_3$ content in the investigated BSLB0- BSLB20 glasses. The BSLB20 glasses presented the least BF (EBF and EABF) at all considered thicknessBased on the $\Sigma_R$ results, the best fast neutron shield among the glasses is the BSLB20 sample. Throughout the entire kinetic energy spectrum, the TSP follows the trend $(TSP)_{BSLB0} < (TSP)_{BSLB4} < (TSP)_{BSLB8} <$

$(TSP)_{BSLB12} < (TSP)_{BSLB16} < (TSP)_{BSLB20}$. The electron absorbing and hence shielding capacity of the BSLB-glasses improves as their $Bi_2O_3$ content increase.

Generally, results confirm that the examined BSLB-glasses can be applied in fields of linear/nonlinear optical devices and radiation shielding applications.

## ACKNOWLEDGEMENT

## REFERENCES

1. Kamitsos, E.I.  Infrared studies of borate glasses. *Physics and Chemistry of Glasses* **2003**, 4, 79–87.
2. Ali, A.A.; Rammah, Y.S.; Shaaban, M.H. The influence of $TiO_2$ on structural, physical and optical properties of $B_2O_3$ - $TeO_2$ - $Na_2O$ - CaO glasses. *J. Non-Cryst. Solids* **2019**, 514, 52–59.
3. Rammah, Y.S.; El-Agwany, F.I.; Mahmoud, K.A.; Novatski, A.; El-Mallawany, R. Role of ZnO on $TeO_2$. $Li_2O$. ZnO glasses for optical and nuclear radiation shielding applications utilizing MCNP5 simulations and WinXCOM program. *J. Non-Cryst. Solids* **2020**, 544, 120162.
4. Rammah, Y.S.; El-Agawany, F.I.; Mahmoud, K.A.; El-Mallawany, R.; Ilik, E.; Kilic, G. FTIR, UV–Vis–NIR spectroscopy, and gamma rays shielding competence of novel ZnO-doped vanadium borophosphate glasses. *J. Mater. Sci.: Mater. Electro.* **2020**, 31, 9099–9113.
5. Rammah, Y.S.; Kilic, G.; El-Mallawany, R.; Issever, U.G.; El-Agawany, F.I. Investigation of optical, physical, and gamma-ray shielding features of novel vanadyl boro-phosphate glasses. *J. Non-Cryst. Solids* **2020**, 533, 119905.
6. Kaewjaeng, S.; Kaewkhao, J.; Limsuwan, P.; Maghanemi, U. Effect of BaO on optical, physical and radiation shielding properties of $SiO_2$-$B_2O_3$-$Al_2O_3$-CaO-$Na_2O$ glasses system. *Proc. Eng.* **2012**, 32, 1080–1086.
7. Sayyed, M.I.; Rashad, M.; Rammah, Y.S. Impact of $Ag_2O$ on linear, nonlinear optical and gamma-ray shielding features of ternary silver vanadio-tellurite glasses: $TeO_2$-$V_2O_5$-$Ag_2O$. *Ceram. Int.* **2020**, 46, 22964–22972.
8. Rammah, Y.S.; Sayyed, M.I.; Ali, A.A.; Tekin, H.O.; El-Mallawany, R. Optical properties and gamma-shielding features of bismuth borate glasses. *Appl. Phys. A* **2018**, 124, 832.
9. Souri, D.; Tahan, Z.E. A new method for the determination of optical band gap and the nature of optical transitions in semiconductors, *Appl. Phys. B* **2015**, 119, 273–279.
10. Martins Jr., A.L., Feitosa, C.A.C.; Santos, W.Q.; Jacinto, C.; Santos, C.C. Influence of $BaX_2$ (X = Cl, F) and $Er_2O_3$ concentration on the physical and optical properties of barium borate glasses. *Phys. B: Condens. Matter* **2019**, 558, 146–153.
11. Kindrat, I.I.; Padlyak, B.V.; Lisiecki, R.; Adamiv, V.T. Optical spectroscopy and luminescence properties of a $Tm^{3+}$-doped $LiKB_4O_7$ glass. *J. Non-Cryst. Solids* **2019**, 521, 119477.
12. Kaur, K.; Singh, K.J.; Anand, V. Correlation of gamma ray shielding and structural properties of PbO-BaO-$P_2O_5$ glass system. *Nucl. Eng. Des.* **2015**, 285, 31–38.
13. Bootjomchai, C.; Laopaiboon, J.; Yenchai, C.; Laopaiboon, R. Gamma-ray shielding and structural properties of barium-bismuth-borosilicate glasses. *Radiat. Phys. Chem.* **2012**, 81, 785–790.

14. Issa, S.; Sayyed, M.; Kurudirek, M. Investigation of gamma radiation shielding properties of some zinc tellurite glasses. *J. Phys. Sci.* **2016**, 27, 97–119.
15. Issa, S.A.M.; Hamdalla, T.A.; Darwish. A.A.A. Effect of $ErCl_3$ in gamma and neutron parameters for different concentration of $ErCl_3$-$SiO_2$ (EDFA) for the signal protection from nuclear radiation. *J. Alloys Compd.* **2017**, 698, 234–240
16. Marzouk, M.A.; ElBatal, H.A.; Abdel Ghany, A.M.; Ezz Eldin, F.M. Ultraviolet, visible, ESR, and infrared spectroscopic studies of $CeO_2$-doped lithium phosphate glasses and effect of gamma irradiation. *J. Mol. Struc.* **2011**, 997, 94–102.
17. El-Batal, F.H.; Khalil, E. M.; Hamdy, Y.M.; Zidan, H.M.; Aziz, M.S.; Abdelghany, A.M. FTIR spectral analysis of corrosion mechanisms in soda lime silica glasses doped with transition metal oxides. *Silicon* **2010**, 2, 41–47.
18. Mortada, W.I.; Kenawy, I.M.M.; Abdelghany, A.M.; Ismail, A.M.; Donia, A.F.; Nabieh, K.A. Determination of $Cu^{2+}$, $Zn^{2+}$ and $Pb^{2+}$ in biological and food samples by FAAS after preconcentration with hydroxyapatite nanorods originated from eggshell. *Mater. Sci. Eng. C* **2015**, 52, 288–296.
19. Hammad, A.H.; Abdelghany, A.M. Optical and structural investigations of zinc phosphate glasses containing vanadium ions. *J. Non-Cryst. Solids* **2016**, 433, 14–19.
20. Abdelghany, A.M.; Rammah, Y.S. Transparent alumino lithium borate glass-ceramics: Synthesis, structure and gamma-ray shielding attitude. *J. Inorg. Organomet. Polym. Mater.* **2021**, 31, 2560–2568.
21. ElBatal, F.H.; Abdelghany, A.M.; ElBatal, H.A. Characterization by combined optical and FT infrared spectra of 3d-transition metal ions doped-bismuth silicate glasses and effects of gamma irradiation. *Spectrochim. Acta Part A: Mol. Biomol. Spectrosc.* **2014**, 122, 461–468.
22. Sayyed, M.I.; Tekin, H.O.; Kılıcoglu, O.; Agar, O.; Zaid, M.H.M. Shielding features of concrete types containing sepiolite mineral: comprehensive study on experimental, XCOM and MCNPX results. *Results Phys.* **2018**, 11, 40–45.
23. El-Agawany, F.I.; Kavaz, E.; Perişanoğlu, U.; Al-Buriahi, M.S.; Rammah, Y.S. $Sm_2O_3$ effects on mass stopping power/projected range and nuclear shielding characteristics of $TeO_2$-ZnO glass systems. *Appl. Phys. A* **2019**, 125, 838.
24. Sayyed, M.I. Investigations of gamma ray and fast neutron shielding properties of tellurite glasses with different oxide compositions. *Canad. J. Phys.* **2016**, 94, 1133–1137.
25. Kavaz, E.; Ekinci, N.; Tekin, H.O.; Sayyed, M.I.; Aygün, B.; Perişanoğlu, U. Estimation of gamma radiation shielding qualification of newly developed glasses by using WinXCOM and MCNPX code. *Prog. Nucl. Energy* **2019**, 115, 12–20.
26. Hegazy, H.H.; Al-Buriahi, M.S.; Alresheedi, F.; El-Agawany, F.I.; Sriwunkum, C.; Neffati, R.; Rammah, Y.S. Nuclear shielding properties of $B_2O_3$-$Bi_2O_3$-SrO glasses modified with $Nd_2O_3$: Theoretical and simulation studies. *Ceram. Int.* **2021**, 47, 2772–2780.
27. Kilic, G.; El Agawany, F.I.; Ilik, B.O.; Mahmoud, K.A.; Ilik, E.; Rammah, Y.S. $Ta_2O_5$ reinforced $Bi_2O_3$–$TeO_2$–ZnO glasses: Fabrication, physical, structural characterization, and radiation shielding efficacy. *Opt.l Mater.* **2021**, 112, 110757.
28. Rammah, Y.S.; Özpolat, Ö.F.; Alım, B.; Şakar, E.; El-Mallawany, R.; El-Agawany, F.I. Assessment of gamma-ray attenuation features for $La^{+3}$ co-doped zinc borotellurite glasses. *Radiat. Phys. Chem.* **2020**, 176, 109069.
29. Rammah, Y.S.; Olarinoye, I.O.; El-Agawany, F.I.; El-Adawy, A.; Yousef, E. The impact of $PbF_2$ on the ionizing radiation shielding competence and mechanical properties of $TeO_2$-$PbF_2$ glasses and glass-ceramics. *Ceram. Int.* **2021**, 47, 2547–2556.
30. Abouhaswa, A.S.; Olarinoye, I.O.; Kudrevatykh, N.V.; Ahmed, E.M.; Rammah, Y.S. $Bi_2O_3$ reinforced $B_2O_3 + Sb_2O_3 + Li_2O$: Composition, physical, linear optical characteristics, and photon attenuation capacity. *J. Mater. Sci: Mater. Electron* **2021**, 32, 12439–12452.

31. Halimah, M.K.; Fazny, M.F.; Azlan, M.N.; Sidek, H.A.A. Optical basicity and electronic polarizability of zinc borotellurite glass doped $La^{3+}$ ions. *Results Phys.* **2017**, 7, 581–589.

32. Umar, S.A.; Halimah, M.K.; Chan, K.T.; Latif, A.A. Polarizability, optical basicity and electric susceptibility of $Er^{3+}$ doped silicate borotellurite glasses. *J. Non-Cryst. Solids* **2017**, 471, 101–109.

33. Duffy, J.A. *Bonding, Energy Level and Bonds in Inorganic Solids*, Longman: England; **1990**.

34. Ticha, H.; Tichy, L. Semiempirical relation between non-linear susceptibility (refractive index), linear refractive index and optical gap and its application to amorphous chalcogenides. *J. Optoelectron. Adv. Mater.* **2002**, 4, 381–386.

35. Olarinoye, I.O. Photon build-up factors for some tissues and phantom materials for penetration depths up to 100 MFP. *J. Nucl. Res. Dev.* **2017**, 13, 57–67.

36. Olarinoye, I.O.; Odiaga, R.I.; Paul, S. EXABCal: A program for calculating photon exposure and energy absorption buildup factors. *Heliyon* **2019**, 5, 02017.

37. Şakar, E.; Özpolat, Ö.F.; Alım, B.; Sayyed, M.I.; Kurudirek, M. Phy-X/PSD: Development of a user friendly online software for calculation of parameters relevant to radiation shielding and dosimetry. *Radiat. Phys. Chem.* **2020**, 166, 108496.

38. Attix, F.H. *Introduction to Radiological Physics and Radiation Dosimetry*, John Wiley and Sons: New York; **2008**.

39. El-Khayatt, A. Calculation of fast neutron removal cross-sections for some compounds and materials. *Ann. Nucl. Energy* **2010**, 37, 218–222.

40. Schmidt, F.A. Attenuation properties of concrete for shielding of neutrons of energy less than 15 MeV (No. ORNL-RSIC-26). Oak Ridge National Lab., Tenn; **1970**.

41. Sears, V.F. Neutron Scattering Lengths and Cross Sections. *Neutron News* **1992**, 3, 29–37.

42. Korkut, T.; Çay, V.V.; Sütçü, M.; Gencel, O. Neutron radiation tests about Fe-Cr slag and natural zeolite loaded brick samples. *Sci. Technol. Nucl. Ins*. **2014**, 190–193.

43. Lakshminarayana, G.; Kebaili, I.; Dong, M.G.; Al-Buriahi, M.S.; Dahshan, A.; Kityk, I.V.; Lee, D-E.; Yoon, J.; Park, T. Estimation of gamma-rays, and fast and the thermal neutrons attenuation characteristics for bismuth tellurite and bismuth boro-tellurite glass systems. *J. Mater. Sci.* **2020**, 55, 5750–5771.

44. Berger, M.J.; Coursey, J.S.; Zucker, M.A.; Chang, J. Stopping-power and range tables for electrons, protons, and helium ions. Gaithersburg, MD: NIST Physics Laboratory; **1998**.

45. Bashter, I.I. Calculation of radiation attenuation coefficients for shielding concretes. *Ann. Nucl. Energy* **1997**, 24, 1389–1401.

46. Akman, F.; Agar, O.; Kacal, M.R.; Sayyed, M.I. Comparison of experimental and theoretical radiation shielding parameters of several environmentally friendly materials. *Nucl. Sci. Tech.* **2019**, 30, 110.

47. Olarinoye, I.O.; El-Agawany, F.I.; El-Adawy, A.; Rammah, Y.S. Mechanical features, alpha particles, photon, proton, and neutron interaction parameters of $TeO_2$-$V_2O_3$-$MoO_3$ semiconductor glasses. *Ceram. Int.* **2020**, 46, 23134–23144.

48. Rammah, Y.S.; Olarinoye, I.O.; El-Agawany, F.I.; El-Adawy, A.; Gamal, A.; Yousef, E. Elastic moduli, photon, neutron, and proton shielding parameters of tellurite bismo-vanadate ($TeO_2$-$V_2O_5$-$Bi_2O_3$) semiconductor glasses. *Ceram. Int.* **2020**, 46, 25440–25452.

49. Tsoulfanidis, N.; Landsberger, S. Measurement and detection of radiation, 4th ed., CRC Press: Taylor and Francis Group, London; **201**; pp. 146, 150, 157.